

Enhanced Hydrogen Evolution Catalysis from Chemically Exfoliated Metallic MoS₂ Nanosheets

Mark A. Lukowski, Andrew S. Daniel, Fei Meng, Audrey Forticaux, Linsen Li, and Song Jin*

Department of Chemistry, University of Wisconsin-Madison, 1101 University Avenue, Madison, Wisconsin 53706, United States

S Supporting Information

ABSTRACT: Promising catalytic activity from molybdenum disulfide (MoS₂) in the hydrogen evolution reaction (HER) is attributed to active sites located along the edges of its two-dimensional layered crystal structure, but its performance is currently limited by the density and reactivity of active sites, poor electrical transport, and inefficient electrical contact to the catalyst. Here we report dramatically enhanced HER catalysis (an electrocatalytic current density of 10 mA/cm² at a low overpotential of −187 mV vs RHE and a Tafel slope of 43 mV/decade) from metallic nanosheets of 1T-MoS₂ chemically exfoliated via lithium intercalation from semiconducting 2H-MoS₂ nanostructures grown directly on graphite. Structural characterization and electrochemical studies confirmed that the nanosheets of the metallic MoS₂ polymorph exhibit facile electrode kinetics and low-loss electrical transport and possess a proliferated density of catalytic active sites. These distinct and previously unexploited features of 1T-MoS₂ make these metallic nanosheets a highly competitive earth-abundant HER catalyst.

The vision of utilizing hydrogen as a future energy carrier requires cost-effective, sustainable, and efficient H₂ production.¹ While Pt and other precious metals are the best catalysts for the hydrogen evolution reaction (HER) in acidic media, replacing rare and expensive electrocatalysts with earth-abundant materials would represent a significant step toward making H₂ a competitive alternative energy source and facilitate the transition to a hydrogen economy.^{1b,2} Although traditionally used as an industrial hydrodesulfurization catalyst,³ molybdenum disulfide (MoS₂) is an exciting HER catalyst⁴ that exhibits promising HER activity in crystalline⁵ or amorphous materials⁶ and molecular mimics.⁷ However, its catalytic HER performance is currently limited by the density and reactivity of active sites, poor electrical transport, and inefficient electrical contact to the catalyst.^{4,6a}

MoS₂ belongs to a large family of two-dimensional (2D) layered metal chalcogenide materials that have the general formula MX₂, where M is a metal and X is a chalcogen (S, Se, or Te). Similar to the graphene layers in graphite, individual sandwiched S–Mo–S layers are held together by weak van der Waals interactions in hexagonally packed structures. Experimental^{5a} and computational^{5b} studies have concluded that the catalytic activity arises from active sites located along the edges of 2D MoS₂ layers, while the basal surfaces are catalytically inert. The edges of MX₂ are undercoordinated and thermodynamically

unfavorable, which explains the general propensity of MX₂ to form closed-shell inorganic fullerene structures when synthesized on the nanoscale.⁸ Recent studies sought to control the MoS₂ nanostructure growth and engineer the surface to maximize the density of active edge sites for catalysis.⁹ Although the number of edge sites is unquestionably important for catalytic performance, as-synthesized MoS₂ is a semiconductor whose poor bulk conduction and anisotropic electrical transport can limit overall catalytic efficiency.^{5a,9a}

However, MoS₂ and other 2D metal chalcogenides can exist in various polymorphs [Figure S1 in the Supporting Information (SI)], wherein subtle structural changes can dramatically affect the electrical properties.¹⁰ Natural MoS₂ is found as the semiconducting and thermodynamically favored 2H phase, which is described by two S–Mo–S layers built from edge-sharing MoS₆ trigonal prisms. In contrast, the metallic 1T polymorph is described by a single S–Mo–S layer composed of edge-sharing MoS₆ octahedra, and it is not naturally found in bulk. Interesting optical and semiconducting properties¹¹ are driving the contemporary research on single layers of semiconducting MX₂ isolated by mechanical¹² or chemical¹³ exfoliation for applications in high-performance devices. Although the 1T-MX₂ structure was characterized during the early exploration of 2D materials,¹⁴ the catalytic HER properties of exfoliated 1T-MoS₂ nanosheets remain unexplored.^{11b} In this work, we were able to overcome the challenges limiting the catalytic performance of MoS₂ by controlling the synthesis of its nanostructures and structural polymorphs using simple intercalation chemistry to make MoS₂ nanostructures a highly competitive earth-abundant catalyst for the HER.

We first synthesized flowerlike MoS₂ nanostructures with a high density of exposed edges directly on graphite substrates via a simple chemical vapor deposition method starting from MoCl₅ and elemental sulfur precursors (see the SI). The relatively mild reaction conditions at 525 °C enabled high-density deposition of MoS₂ nanostructures on a variety of substrates, including silicon/silicon oxide, glass, fluorine-doped tin oxide on glass, Mo foils, carbon paper, and graphite (Figure S2). This highly tunable synthesis¹⁵ offers two advantages: (i) the dense MoS₂ flakes are dominated by edges (Figure 1a), thus increasing the density of active sites, and (ii) the direct growth on conductive graphite substrates results in high-quality, low-electrical-loss contact to the 3D nanostructured electrocatalyst (Figure 1b). Transmission electron microscopy (TEM) confirmed that the as-grown nanostructures were multilayered open structures (not inorganic

Received: May 6, 2013

Published: June 21, 2013

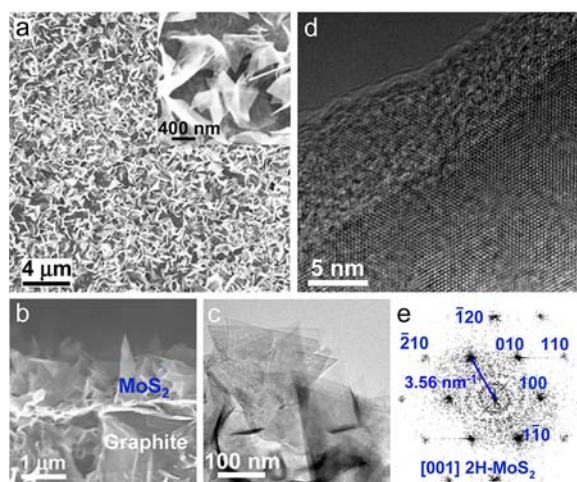


Figure 1. Electron microscopy characterization of as-grown 2H-MoS₂ nanostructures. (a) Top-down and (b) cross-sectional SEM images. (c) Low-resolution TEM image. (d) HRTEM image with (e) the corresponding indexed FFT pattern.

fullerenes) with widths of hundreds of nanometers (Figure 1c). The lattice-resolved high-resolution TEM (HRTEM) image (Figure 1d) and the corresponding fast Fourier transform (FFT) pattern (Figure 1e) showed highly crystalline structures that were indexed unequivocally to 2H-MoS₂.

We further confirmed the phase identity of the as-synthesized MoS₂ nanostructures using powder X-ray diffraction (PXRD) (Figure 2a) and Raman spectroscopy (Figure 2b). Strong (00 l) reflections in the PXRD pattern illustrated the crystallinity and ordered stacking of the 2D layers in the as-grown MoS₂ nanostructures. Scherrer analysis of the peak broadening in the (002) reflection yielded an estimated average of 12 MoS₂ layers per flake. The characteristic Raman shifts at 387, 412, and 456 cm⁻¹ expected for the E_{2g}, A_{1g}, and longitudinal acoustic phonon modes, respectively, of 2H-MoS₂¹⁶ were clearly observed.

We then converted the as-grown multilayered semiconducting MoS₂ nanostructures into the metallic 1T-MoS₂ polymorph by simply soaking them in *n*-butyllithium solution at room temperature or 60 °C for 6–48 h, and then exfoliating the nanostructures by reacting the intercalated lithium with excess water, which generated H₂ gas and separated the 2D nanosheets (see the SI). The absence of the (00 l) peaks in the PXRD pattern of an exfoliated sample (Figure 2a, top trace) clearly showed that the long-range stacking order of the nanosheets along the *c* axis was destroyed, indicating that the MoS₂ nanostructures were efficiently exfoliated into essentially single layers of MoS₂. These structures are called MoS₂ nanosheets. It should be noted that lithium intercalation into graphite is not favorable under these conditions.¹⁷ The transition to the 1T phase is caused by electron transfer from intercalated Li, which destabilizes the original trigonal-prismatic 2H-MoS₂ structure and favors octahedrally coordinated Mo atoms.^{10a} The emergence of new Raman shifts at 150, 219, and 327 cm⁻¹ associated with the phonon modes of 1T-MoS₂ (Figure 2b, bottom trace)^{10c,16} clearly confirmed the formation of 1T-MoS₂ in the exfoliated nanosheets. The Raman shifts associated with the 2H phase were significantly suppressed but still observed. Although this exfoliation method is known to yield primarily 1T-MoS₂,^{10a,13a} recent studies showed the coexistence of coherent nanometer-sized domains of the 1T and 2H polymorphs in exfoliated single-layer MoS₂.¹⁸ The semiconducting-to-metallic phase transition was also confirmed

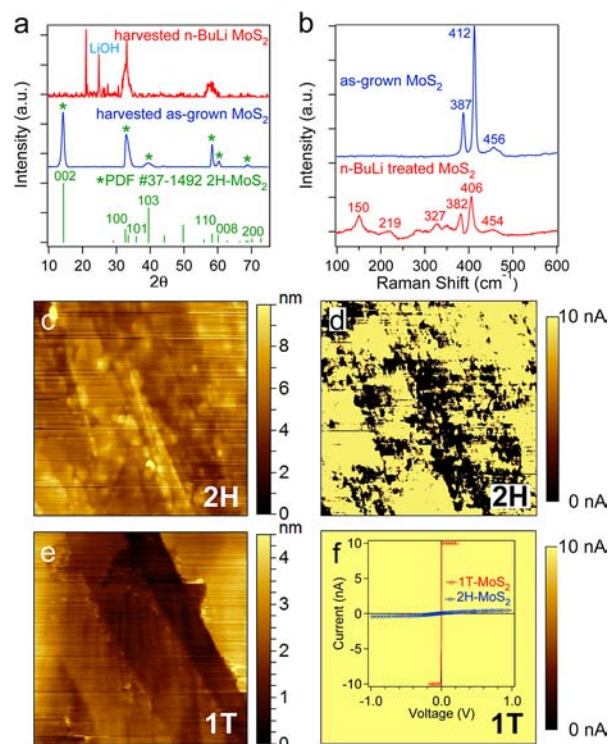


Figure 2. Comparison of as-grown and exfoliated MoS₂ nanosheets. (a) PXRD patterns and (b) Raman spectra illustrating that the as-grown sample is pure 2H-MoS₂ and the exfoliated MoS₂ nanosheets contain a mixture of 1T- and 2H-MoS₂. (c, e) CSAFM micrographs and (d, f) conductivity maps for (c, d) as-grown and (e, f) chemically exfoliated MoS₂ nanosheets. All of the images are 3 μm × 3 μm, and the conductivity maps were taken at a bias of 50 mV. Superimposed on the conductivity map in (f) is a plot showing the results of individual current–voltage sweeps on specific nanostructures.

by current-sensing atomic force microscopy (CSAFM). Contact-mode topography (Figure 2c,e) and friction and deflection images (Figure S3) clearly showed the presence of material on a highly ordered pyrolytic graphite (HOPG) substrate. The corresponding conductivity maps taken at +50 mV sample bias revealed the uniformly metallic conduction in the exfoliated MoS₂ (Figure 2f) and the inhomogeneous conductivity in the semiconducting 2H-MoS₂ (Figure 2d). Individual current–voltage sweeps on specific nanostructures (Figure 2f inset) showed the contrast between the relatively poor conductivity of the as-grown 2H-MoS₂ and the metallic conduction observed in the exfoliated MoS₂. The small size (1–10 nm²) expected for the remnant nanodomains of the 2H polymorph present in the chemically exfoliated nanosheets¹⁸ was below the resolution limit of the CSAFM instrument, which had a 30 nm diameter tip.

The MoS₂ nanostructure morphology was preserved after exfoliation (Figure 3a), though the exfoliated nanosheets were more disordered and compressed onto the substrate surface than the as-grown 3D MoS₂ nanoflowers (Figure 1a). Cross-sectional scanning electron microscopy (SEM) (Figure 3b) suggested that electrical contact between the electrocatalyst and the graphite substrate was maintained after exfoliation. HRTEM clearly showed regions of MoS₂ sheets with resolved crystal lattice, but the exfoliated nanosheets quickly became amorphous under the typical 200 kV HRTEM imaging conditions (arrows in Figure 3c). The nanosheets were stable under a lower accelerating voltage of 120 kV (Figure 3d), enabling an electron diffraction (ED) study even though HRTEM imaging was not possible. The

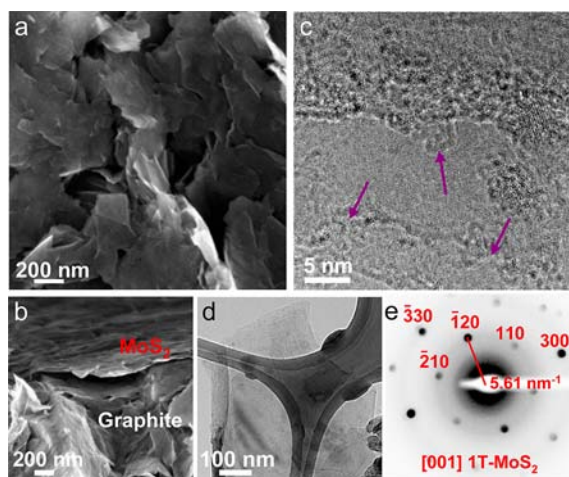


Figure 3. Electron microscopy characterization of chemically exfoliated MoS₂ nanosheets. (a) Top-down and (b) cross-sectional SEM images. (c) Unstable HRTEM image taken at 200 kV. (d) Stable TEM image taken at 120 kV and (e) the corresponding indexed ED pattern.

indexed [001] zone axis ED pattern (Figure 3e) confirmed the expected crystal symmetry and expansion of the lattice constant for 1T-MoS₂^{10b} (see the SI and Figure S4 for details).

We found that this simple chemical exfoliation dramatically enhances the catalytic HER performance of MoS₂ nanosheets relative to the as-grown nanostructures. The direct growth and exfoliation of MoS₂ nanosheets on conducting graphite substrates enabled convenient evaluation of their catalytic activity by attachment of the substrate to a standard rotating disk electrode apparatus in a three-electrode electrochemical measurement using a 0.5 M H₂SO₄(aq) electrolyte continuously purged with H₂ (see the SI). Polarization curves of the current density (*J*) plotted against potential showed the HER activity of the as-grown MoS₂ and chemically exfoliated MoS₂ nanosheets on graphite in comparison with Pt (Figure 4a,b). As-grown 2H-MoS₂ exhibited the onset of HER activity near -200 mV vs reversible hydrogen electrode (RHE), consistent with previous reports,^{5a,c,9a} and significant H₂ evolution (*J* = 10 mA/cm²) was not achieved until -320 mV vs RHE. 1T-MoS₂ nanosheets exfoliated after lithium intercalation at 60 °C for 48 h showed dramatically improved HER activity, with *J* reaching 200 mA/cm² at -400 mV vs RHE (Figure 4a). Moreover, the onset of the catalytic activity shifted to a much lower overpotential, as significant H₂ evolution (*J* = 10 mA/cm²) was observed at a voltage as low as -195 mV (Figure 4b). Correcting the raw data for *iR* losses (see the SI and Figure S5) revealed even more impressive performance, as *J* = 10 mA/cm² was achieved at a low overpotential of -187 mV vs RHE (filled squares in Figure 4b). Electrochemical tests on a series of MoS₂ samples synthesized in a single batch but subjected to different lithium intercalation conditions (Figure S6) showed that gentle heating to 60 °C and the use of a more concentrated 2.7 M *n*-BuLi solution accelerated the intercalation process, affording more electrocatalytically active MoS₂ nanosheets in a shorter intercalation time. However, a significant shift in the activity onset could be observed even for MoS₂ nanosheets that were intercalated at room temperature for 6 h. The dramatic enhancement in catalytic activity was even more apparent upon comparison of the slopes of Tafel plots (Figure 4c) for the exfoliated MoS₂ nanosheets (54 mV/decade raw; 43 mV/decade after *iR* correction) and as-grown nanostructures (117 mV/decade; 110 mV/decade after *iR*

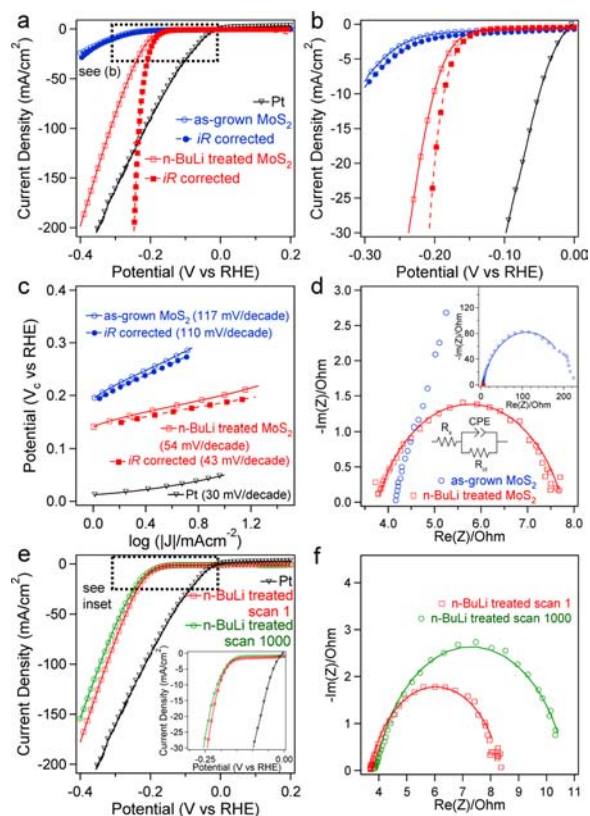


Figure 4. Electrocatalytic performance of chemically exfoliated and as-grown MoS₂ nanosheets. (a, b) Polarization curves at (a) higher and (b) lower potentials and (c) corresponding Tafel plots. Filled symbols show *iR*-corrected data. (d) Nyquist plots showing the facile electrode kinetics of 1T-MoS₂. (e) Polarization curves and (f) Nyquist plots showing that 1T-MoS₂ nanosheets still exhibited excellent catalytic activity after 1000 cycles of continuous operation.

correction). The earlier onset of catalytic activity and smaller Tafel slope suggest that the hydrogen adsorption is closer to equilibrium. The 43 mV/decade Tafel slope and the early onset of significant H₂ evolution confirm that 1T-MoS₂ is among the most catalytic MoS₂ materials.⁴

Although the efficient exfoliation of MoS₂ nanoflowers (Figure 2a) results in the proliferation of active edge sites, we believe that the phase transition into the metallic 1T polymorph is even more important in enhancing the catalytic activity. The increase in the density of active sites due to exfoliation was revealed by the >10-fold increase in the double-layer capacitance (*C_{dl}*) and thus the relative electrochemical surface area as estimated using a simple cyclic voltammetry method¹⁹ (Figure S7). However, exfoliated semiconducting 2H-MoS₂ nanosheets were recently investigated for H₂ evolution and showed only marginally improved catalytic performance,²⁰ suggesting that the density of edge sites is not the most important factor underlying the dramatically enhanced performance of our 1T-MoS₂ nanosheets. Interestingly, the edges of 2H-MoS₂ have been observed to be more conductive and posited to be inherently more catalytically active.^{4,5} However, practical implementation of metallic 1T-MoS₂ has not been pursued. Although exfoliated MoS₂ has been investigated for hydrodesulfurization catalysis,²¹ the high-temperature conditions cause its quick conversion back to the 2H phase, since 1T-MoS₂ is metastable only below 95 °C.^{10b} Here, the phase identity and metallic conduction of 1T-MoS₂ were confirmed by Raman spectroscopy (Figure 2b), ED (Figure

3e), and CSAFM (Figure 2f). The advantage of the 1T-MoS₂ nanosheets became more apparent when we used electrochemical impedance spectroscopy (EIS) to investigate the electrode kinetics under HER operating conditions. Nyquist plots (Figure 4d) revealed a dramatically decreased charge-transfer resistance (R_{CT}) for the exfoliated MoS₂ nanosheets (4 Ω) relative to the as-grown MoS₂ nanostructures (232 Ω). Furthermore, the small series resistances observed for all samples (~4 Ω) shows the importance of the direct synthesis on conductive substrates, which enables simple and effective electrical integration that minimized parasitic Ohmic losses.²² The structural characterization and EIS results show that exfoliated metallic 1T-MoS₂ nanosheets exhibit more facile electrode kinetics, a particularly useful feature in enhancing the catalytic activity that was not realized in previous efforts to improve MoS₂ for HER catalysis.^{4–7,9}

Furthermore, we demonstrated that the catalytic performance of 1T-MoS₂ nanosheets is stable even though the 1T-phase is thermodynamically metastable. After 1000 cycles of continuous operation, exfoliated MoS₂ nanosheets showed <15% decay in the electrocatalytic current density (Figure 4e). Further EIS studies (Figure 4f) showed that the slight loss in catalytic activity was accompanied by a slight increase in R_{CT} . Additional stability tests showed that the overpotential required to sustain a constant current density of 10 mA/cm² increased by only 10 mV after 9 h of continuous service (Figure S8). The minimal loss in catalytic activity suggested that the metallic 1T polymorph slowly reverted to the semiconducting 2H phase. This hypothesis was further supported by longer phase-stability studies in which we monitored the HER activity of exfoliated MoS₂ nanosheets aged over 3 weeks under ambient conditions (Figure S9).

In conclusion, we have demonstrated a simple and rational method to provide a significant enhancement of the electrocatalytic performance of MoS₂ by controlling its nanostructures and structural polymorphs using chemical exfoliation. This new approach leads to favorable kinetics, metallic conductivity, and proliferation of active sites in the exfoliated 1T-MoS₂ nanosheets, which enable superior yet stable catalytic activity and make MoS₂ nanostructures a highly competitive earth-abundant catalyst for HER and potentially other reactions. Furthermore, this represents the first application of the metallic 1T polymorph of layered metal chalcogenides in catalysis, and this general approach for controlling nanostructures and polymorphism can be useful in modifying many 2D layered materials to enhance their applications in heterogeneous catalysis, solar energy, and high-performance electronics.

■ ASSOCIATED CONTENT

Supporting Information

Experimental details and supporting figures. This material is available free of charge via the Internet at <http://pubs.acs.org>.

■ AUTHOR INFORMATION

Corresponding Author

jin@chem.wisc.edu

Notes

The authors declare no competing financial interest.

■ ACKNOWLEDGMENTS

This research was supported by the U.S. Department of Energy, Office of Basic Energy Sciences, Division of Materials Sciences and Engineering, under Award DE-FG02-09ER46664. S.J. is also

grateful for support through a Research Corporation Scialog Award and the UW-Madison Vilas Associate Award.

■ REFERENCES

- (1) (a) Turner, J. A. *Science* **2004**, *305*, 972. (b) Lewis, N. S.; Nocera, D. G. *Proc. Natl. Acad. Sci. U.S.A.* **2006**, *103*, 15729.
- (2) McKone, J. R.; Warren, E. L.; Bierman, M. J.; Boettcher, S. W.; Brunschwig, B. S.; Lewis, N. S.; Gray, H. B. *Energy Environ. Sci.* **2011**, *4*, 3573.
- (3) Chianelli, R. R.; Siadati, M. H.; De la Rosa, M. P.; Berhault, G.; Wilcoxon, J. P.; Bearden, R.; Abrams, B. L. *Catal. Rev.* **2006**, *48*, 1.
- (4) Laursen, A. B.; Kegnaes, S.; Dahl, S.; Chorkendorff, I. *Energy Environ. Sci.* **2012**, *5*, 5577.
- (5) (a) Jaramillo, T. F.; Jørgensen, K. P.; Bonde, J.; Nielsen, J. H.; Horch, S.; Chorkendorff, I. *Science* **2007**, *317*, 100. (b) Hinnemann, B.; Moses, P. G.; Bonde, J.; Jørgensen, K. P.; Nielsen, J. H.; Horch, S.; Chorkendorff, I.; Nørskov, J. K. *J. Am. Chem. Soc.* **2005**, *127*, 5308. (c) Bonde, J.; Moses, P. G.; Jaramillo, T. F.; Nørskov, J. K.; Chorkendorff, I. *Faraday Discuss.* **2009**, *140*, 219. (d) Li, Y.; Wang, H.; Xie, L.; Liang, Y.; Hong, G.; Dai, H. *J. Am. Chem. Soc.* **2011**, *133*, 7296. (e) Vrubel, H.; Merki, D.; Hu, X. *Energy Environ. Sci.* **2012**, *5*, 6136.
- (6) (a) Merki, D.; Fierro, S.; Vrubel, H.; Hu, X. *Chem. Sci.* **2011**, *2*, 1262. (b) Benck, J. D.; Chen, Z.; Kuritzky, L. Y.; Forman, A. J.; Jaramillo, T. F. *ACS Catal.* **2012**, *2*, 1916.
- (7) Karunadasa, H. I.; Montalvo, E.; Sun, Y.; Majda, M.; Long, J. R.; Chang, C. J. *Science* **2012**, *335*, 698.
- (8) Tenne, R.; Redlich, M. *Chem. Soc. Rev.* **2010**, *39*, 1423.
- (9) (a) Kibsgaard, J.; Chen, Z.; Reinecke, B. N.; Jaramillo, T. F. *Nat. Mater.* **2012**, *11*, 963. (b) Kong, D.; Wang, H.; Cha, J. J.; Pasta, M.; Koski, K. J.; Yao, J.; Cui, Y. *Nano Lett.* **2013**, *13*, 1341.
- (10) (a) Py, M. A.; Haering, R. R. *Can. J. Phys.* **1983**, *61*, 76. (b) Wypych, F.; Schollhorn, R. *J. Chem. Soc., Chem. Commun.* **1992**, 1386. (c) Yang, D.; Sandoval, S. J.; Divigalpitiya, W. M. R.; Irwin, J. C.; Frindt, R. F. *Phys. Rev. B* **1991**, *43*, 12053.
- (11) (a) Wang, Q. H.; Kalantar-Zadeh, K.; Kis, A.; Coleman, J. N.; Strano, M. S. *Nat. Nanotechnol.* **2012**, *7*, 699. (b) Chhowalla, M.; Shin, H. S.; Eda, G.; Li, L.-J.; Loh, K. P.; Zhang, H. *Nat. Chem.* **2013**, *5*, 263.
- (12) Novoselov, K. S.; Jiang, D.; Schedin, F.; Booth, T. J.; Khotkevich, V. V.; Morozov, S. V.; Geim, A. K. *Proc. Natl. Acad. Sci. U.S.A.* **2005**, *102*, 10451.
- (13) (a) Joensen, P.; Frindt, R. F.; Morrison, S. R. *Mater. Res. Bull.* **1986**, *21*, 457. (b) Coleman, J. N.; Lotya, M.; O'Neill, A.; Bergin, S. D.; King, P. J.; Khan, U.; Young, K.; Gaucher, A.; De, S.; Smith, R. J.; Shvets, I. V.; Arora, S. K.; Stanton, G.; Kim, H.-Y.; Lee, K.; Kim, G. T.; Duesberg, G. S.; Hallam, T.; Boland, J. J.; Wang, J. J.; Donegan, J. F.; Grunlan, J. C.; Moriarty, G.; Shmeliov, A.; Nicholls, R. J.; Perkins, J. M.; Grievson, E. M.; Theuwissen, K.; McComb, D. W.; Nellist, P. D.; Nicolosi, V. *Science* **2011**, *331*, 568.
- (14) Murphy, D. W.; Di Salvo, F. J.; Hull, G. W.; Waszczak, J. V. *Inorg. Chem.* **1976**, *15*, 17.
- (15) (a) Bierman, M. J.; Lau, Y. K. A.; Kvit, A. V.; Schmitt, A. L.; Jin, S. *Science* **2008**, *320*, 1060. (b) Lau, Y. K. A.; Chernak, D. J.; Bierman, M. J.; Jin, S. *J. Am. Chem. Soc.* **2009**, *131*, 16461.
- (16) Sandoval, S. J.; Yang, D.; Frindt, R. F.; Irwin, J. C. *Phys. Rev. B* **1991**, *44*, 3955.
- (17) Benavente, E.; Santa Ana, M. A.; Mendizábal, F.; González, G. *Coord. Chem. Rev.* **2002**, *224*, 87.
- (18) Eda, G.; Fujita, T.; Yamaguchi, H.; Voiry, D.; Chen, M.; Chhowalla, M. *ACS Nano* **2012**, *6*, 7311.
- (19) Merki, D.; Vrubel, H.; Rovelli, L.; Fierro, S.; Hu, X. *Chem. Sci.* **2012**, *3*, 2515.
- (20) Ge, P.; Scanlon, M. D.; Peljo, P.; Bian, X.; Vubrel, H.; O'Neill, A.; Coleman, J. N.; Cantoni, M.; Hu, X.; Kontturi, K.; Liu, B.; Girault, H. H. *Chem. Commun.* **2012**, *48*, 6484.
- (21) Miremedi, B. K.; Morrison, S. R. *J. Catal.* **1987**, *103*, 334.
- (22) Faber, M. S.; Park, K.; Cabán-Acevedo, M.; Santra, P. K.; Jin, S. *J. Phys. Chem. Lett.* **2013**, *4*, 1843.